Journal of Solid State Electrochemistry (2018) 22:2989–2998
https://doi.org/10.1007/s10008-018-4010-3

ORIGINAL PAPER

Lithium garnet based free-standing solid polymer composite membrane for rechargeable lithium battery

K. Karthik[1] · Ramaswamy Murugan[1]

Received: 2 February 2018 / Revised: 11 May 2018 / Accepted: 30 May 2018 / Published online: 7 June 2018

Abstract

Electrolytes with high lithium-ion conductivity, better mechanical strength and large electrochemical window are essential for the realization of high-energy density lithium batteries. Polymer electrolytes are gaining interest due to their inherent flexibility and nonflammability over conventional liquid electrolytes. In this work, lithium garnet composite polymer electrolyte membrane (GCPEM) consisting of large molecular weight ($W_{avg} \sim 5 \times 10^6$) polyethylene oxide (PEO) complexed with lithium perchlorate ($LiClO_4$) and lithium garnet oxide $Li_{6.28}Al_{0.24}La_3Zr_2O_{12}$ (Al-LLZO) is prepared by solution-casting method. Significant improvement in Li^+ conductivity for Al-LLZO containing GCPEM is observed compared with the Al-LLZO free polymer membrane. Maximized room temperature (30 °C) Li^+ conductivity of 4.40×10^{-4} S cm^{-1} and wide electrochemical window (4.5 V) is observed for $PEO_8/LiClO_4$ + 20 wt% Al-LLZO (GCPEM-20) membrane. The fabricated cell with $LiCoO_2$ as cathode, metallic lithium as anode and GCPEM-20 as electrolyte membrane delivers an initial charge/discharge capacity of 146 mAh g^{-1}/ 142 mAh g^{-1} at 25 °C with 0.06 C-rate.

Keywords Lithium garnet · Solid polymer electrolyte · Ionic conductivity · Lithium metal battery

Introduction

In recent times an intensive research activities have been focused to develop lithium-ion batteries (LIBs) with high energy density and long cycle life. The commercial Li^+ batteries containing organic liquid electrolytes frequently suffered from potential safety risks due to leakage, volatility, limited temperature range of operation and spontaneous combustion of the electrolyte. Polymer electrolytes (PEs) were found to be an alternative approach for Li^+ batteries [1–6]. Li^+ batteries comprising polymer electrolyte offers enhanced electrode/electrolyte compatibility, high flexibility, and simple technological process [7].

PEO-based polymer electrolytes have been studied widely due to their outstanding film-forming ability and relatively better compatibility towards electrodes. PEO contains multiple polymeric chains of ether oxygen capable of forming coordination bonds with metal ions from the lithium salts. PEO is a semicrystalline polymer at room temperature which has the capacity to dissolve high concentration of metal salts. It has been reported well that the amorphous phase supports the conduction mechanism when compared with the crystalline domains. The major downside of PEO-based polymer electrolytes is that they exhibit low ionic conductivity (10^{-6} to 10^{-8} S cm^{-1}) at room temperature. The ionic conductivity in PEO-based electrolytes has been improved by polymer blending and incorporating fillers such as TiO_2, SiO_2, Al_2O_3, ZnO, $BaTiO_3$, $PbTiO_3$, and $LiNbO_3$ into the polymer matrix [8–10]. The polymer blends offers superior ionic conductivity than that of the electrolytes based on individual polymer [11]. The dispersion of nano/microfillers in PEO hosts not only improves the ionic conductivity but also enhances the mechanical and electrochemical stability [12, 13]. Movement of Li^+ in PEO chains arise due to the breaking and reformation of ether oxygen with complexes. The segmental motion of the polymer assists this transport mechanism [14, 15].

Free-standing composite polymer membranes comprising of lithium garnet as a constituent received considerable attention [16, 17]. Recently, Zheng et al. demonstrated that the Li^+ preferred to diffuse through the cubic phase $Li_7La_3Zr_2O_{12}$ (LLZO) garnet rather than the polymer-garnet interphase or the PEO polymer phase [18].

✉ Ramaswamy Murugan
moranamurugan.phy@pondiuni.edu.in

[1] High Energy Density Batteries Research Laboratory, Department of Physics, Pondicherry University, Puducherry 605 014, India

In this work, lithium garnet solid composite polymer electrolyte membrane (GCPEM) consisting of a large molecular weight ($W_{avg} \sim 5 \times 10^6$) polyethylene oxide (PEO) complexed with lithium perchlorate ($LiClO_4$) and lithium garnet oxide $Li_{6.28}Al_{0.24}La_3Zr_2O_{12}$ (Al-LLZO) were prepared by solution-casting method. To optimize the system, we have varied the composition of PEO/$LiClO_4$ and it was optimized at the ratio of 8:1. Among the various compositions, the PEO_8/$LiClO_4$ membrane exhibits maximized Li^+ conductivity. Detailed study on the optimization has been reported in our previous work [19]. Also, we varied the Al-LLZO content as 0, 5, 10, 15, 20, 25, and 30 wt% in PEO_8/$LiClO_4$. Maximized room temperature Li^+ conductivity was observed for PEO_8/$LiClO_4$ + 20 wt% Al-LLZO (GCPEM-20) membrane. The cell fabricated with GCPEM-20 as electrolyte, $LiCoO_2$ as cathode and metallic Li anode delivered an initial charge/discharge capacity of 146 mAh g^{-1}/142 mAh g^{-1} at 25 °C with 0.06 C-rate.

Experimental details

Preparation of GCPEM and $LiCoO_2$ tape

Preparation of GCPEM

$Li_{6.2}Al_{0.24}La_3Zr_2O_{12}$ (Al-LLZO) garnet oxide powder was synthesized by the conventional solid-state method as described earlier [20]. The Al-LLZO pellets prepared by solid-state method were crushed in to powder and again wet ball milled for 6 h and dried. The Malvern Mastersizer2000 instrument has been used to estimate the particle size of the prepared Al-LLZO, and it was found that the size of the grounded Al-LLZO particle was around 343 nm.

The poly(ethylene oxide) (PEO) ($W_{avg} \sim 5 \times 10^6$) and lithium perchlorate ($LiClO_4$) were purchased from Sigma-Aldrich. $LiClO_4$ was dried overnight in the oven at 90 °C prior to use in order remove the moisture content. The PEO/$LiClO_4$ molar ratio was fixed as 8:1 to get the maximized Li^+ conductivity based on our earlier report [19], and the amount of Al-LLZO was varied from 5 to 30 wt% with respect to the total weight of PEO and $LiClO_4$.

To prepare the PEO_8/$LiClO_4$ complex, stoichiometric amount of PEO was dissolved in acetonitrile (ACN) and continuously stirred for 4 h. An appropriate amount of $LiClO_4$ was added to the stirring polymer solution, and stirring was continued for next 4 h. After the complete dissolution of $LiClO_4$ into the polymer, a homogeneous and transparent solution was obtained. The solution was later casted onto a cleaned glass petri dish.

In order to synthesize Al-LLZO garnet oxide dispersed composite membrane (GCPEM), an appropriate amount of finely grounded Al-LLZO garnet oxide (0, 5, 10, 15, 20, 25, and 30 wt% in PEO_8/$LiClO_4$) was added to ACN and ultrasonicated for 45 min. The ultrasonicated Al-LLZO solution was mixed to the PEO_8/$LiClO_4$ solution and stirred for 6 h to achieve a homogeneous viscous solution then casted onto a glass petri dish. The ACN component was then slowly evaporated from the casted solutions at room temperature inside the argon filled glove box (oxygen and moisture levels maintained at ≤ 1 ppm). After complete drying, thin GCPEM with thickness ranging from 100 to 150 μm were obtained.

Preparation lithium cobalt oxide ($LiCoO_2$) cathode

Commercial $LiCoO_2$ powder (Sigma-Aldrich), polyvinylidene fluoride (PVDF) binder in N-methyl-2-pyrrolidinone (NMP), and active carbon were mixed together in ratio of 8:1:1, respectively, to prepare the slurry. Using doctor blade, the prepared slurry was tape casted over aluminum foil. The $LiCoO_2$-coated tape (LCO) was initially dried in vacuum oven at 120 °C for 12 h and then hot pressed. Finally, the dried tape was cut in to small disc of required size and used for battery fabrication inside the Ar-filled glove box (oxygen and moisture levels maintained at ≤ 1 ppm).

Characterization

The crystal structure and phase purity of the prepared samples were examined by Rigaku Miniflex II Powder X-ray diffractometer with a characteristic CuKα (λ = 1.54059 Å) radiation in the angle ranging from 10° to 80° at a scan rate of 1° min^{-1}. The formation of polymer–salt complexes and interaction between salt and polymer were examined by Fourier transform infrared spectroscopy (FTIR) using Jasco FT/IR-6300 spectrometer in the wavenumber region of 1600–500 cm^{-1}. The Li^+ conductivity measurements of prepared GCPEM were performed using Li^+ blocking stainless steel electrodes in the frequency range 20 Hz to 15 MHz using a Wayne Kerr 6500B precision impedance analyzer. Differential scanning calorimetric analysis (DSC) was performed with METTLER TOLEDO STAR System under air flow with a heating rate of 5 °C min^{-1} in the temperature range from 30 to 150 °C. HITACHI S-3400N scanning electron microscope (SEM) was used to examine the morphology of the prepared polymer films. Transmission electron microscopic (TEM) measurement has been performed with FEI TECNAI T20 G2 instrument. For TEM measurement, the sample has been dissolved in ethanol initially; then, the prepared colloidal solution has been casted onto the carbon-coated copper grid for support during viewing and then dried without exposing to humidity and CO_2 before the TEM analysis. Electrochemical measurements were carried out by using Biologic VMP3

instruments. Cyclic voltammetry (CV) and linear sweep voltammetry (LSV) measurements were carried out using two electrodes system Li/GCPEM-20/SS comprising of a stainless steel as working electrode and metallic lithium as reference/counter electrode. The stability of GCPEM-20 membrane was verified by measuring the galvanostatic cycling with potential limitation (GCPL) measurement of symmetric cell Li/GCPEM-20/Li. The charging and discharging behavior of GCPEM-20 membrane against LCO cathode and metallic lithium anode in CR2032 coin cell was analyzed in a voltage window of 3.0–4.2 V at room temperature.

Results and discussion

X-ray diffraction (XRD)

The X-ray diffraction pattern of PEO and $PEO_8/LiClO_4$ are shown as Fig. 1a, b, respectively. The diffraction peaks observed at $2\theta = 19°$ and 23° in Fig. 1a corresponds to the prominent crystalline peaks of PEO [21]. The addition of lithium salt into the polymer decreases the intensity of the characteristic peaks of PEO which reveals the dissolution of lithium ions into the PEO chains. An amorphous halo observed around $2\theta = 15°–25°$ in Fig. 1b arises due to the short-range order, which is used as template in analyzing the diffraction pattern of $PEO_8/LiClO_4$-Al-LLZO. The peak positions of the amorphous halo at 19° and 23° are related to that of the PEO, but due to the distribution of the bond lengths and bond angles, the broadening of these peaks occurs, which gives the characteristic amorphous halo.

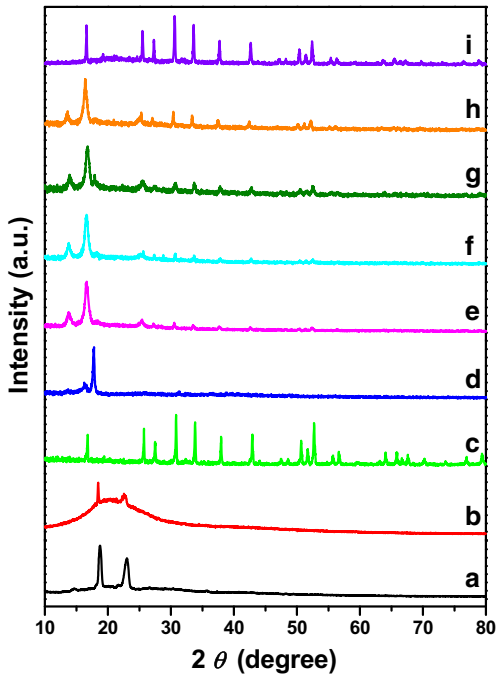

Fig. 1 XRD pattern of (**a**) PEO, (**b**) $PEO_8/LiClO_4$, (**c**) Al-LLZO, and $PEO_8/LiClO_4 + x$ wt% Al-LLZO with (**d**) $x = 5$, (e) $x = 10$, (**f**) $x = 15$, (**g**) $x = 20$, (**h**) $x = 25$, and (**i**) $x = 30$

The measured powder XRD pattern of as-synthesized garnet oxide Al-LLZO in cubic phase ($Ia\bar{3}d$) is shown as Fig. 1c. Generally, the LLZO exist in two phases such as tetragonal phase ($I4_1/acd$) and cubic phase ($Ia\bar{3}d$). It has been already reported that the cubic phase ($Ia\bar{3}d$) exhibits maximized Li^+ conductivity compared to the tetragonal phase [22]. The intensities of PEO diffraction peaks diminished with the incorporation of Al-LLZO garnet oxide into the $PEO_8/LiClO_4$ system. Shift in the diffraction peak at around $2\theta = 15^o$ of PEO was observed with the 5 and 10 wt% loading (Fig. 1d, e) of Al-LLZO and the intensity of this peak decreases with the further loading of Al-LLZO, and later, it has been completely diminished with the higher loading of Al-LLZO (Figs. 1f–i). Addition of Al-LLZO also exhibit slight shift in the diffraction peak of PEO, which might be due to the Lewis acid base interaction between the oxygen atom of polymer and the surface oxygen atom of Al-LLZO. As the weight percentage of Al-LLZO increased beyond 20 wt% the intensity of the diffraction peaks corresponding to the Al-LLZO becomes more prominent as shown in Fig. 1h, i.

Fourier transform infrared spectroscopy (FTIR)

Infrared analysis is a powerful technique to identify the nature of bonding and functional groups present in a sample. FTIR spectroscopy was used to probe the interaction between PEO, $LiClO_4$, and Al-LLZO garnet oxide.

The FTIR spectrum of PEO, $PEO_8/LiClO_4$, and $PEO_8/LiClO_4$ + 20 wt% Al-LLZO (GCPEM-20) membranes in the wave number region from 1600 to 500 cm^{-1} are shown in Figs. 2a–c, respectively. The FTIR spectrum of PEO (Fig. 2a) contains bands at 1466, 1091, and 841 cm^{-1} corresponding to the CH_2 scissoring mode, C-O-C stretching mode, and CH_2 wagging mode, respectively [23]. Figure 2b shows the FTIR spectrum of $PEO_8/LiClO_4$ complex. The modifications observed in the band at C-O-C stretching mode in terms of peak shift, intensity, and bandwidth were induced by the complexation reaction taking place between the lithium ions and the ether oxygen in PEO. The band pertaining to C-O-C stretching mode observed at 1091 cm^{-1} in PEO spectrum (Fig. 2a) is shifted to a lower wave number (1076 cm^{-1}) in the $PEO_8/LiClO_4$ complex (Fig. 2b). The decrease in wave number indicates an increase in C-O-C bond length which confirms the electrostatic interaction occurred between the lithium ions and ether oxygen. This interaction leads to the weakening of C-O-C bond strength [24]. The small bumps which were

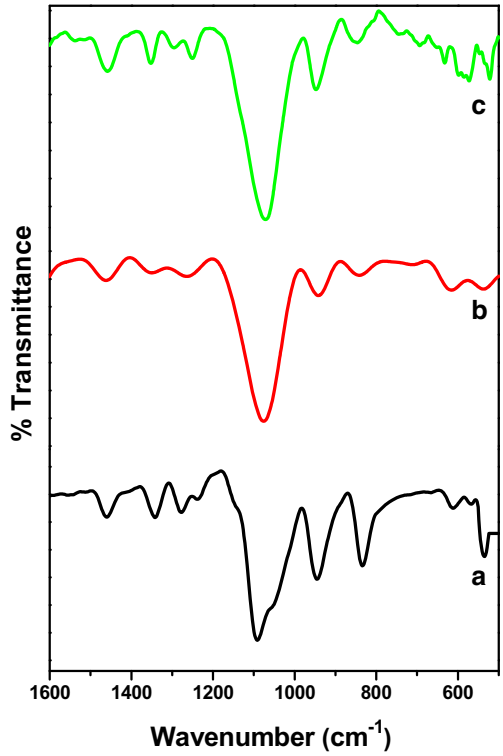

Fig. 2 FTIR spectrum of (**a**) PEO, (**b**) $PEO_8/LiClO_4$, and (**c**) GCPEM-20 membrane

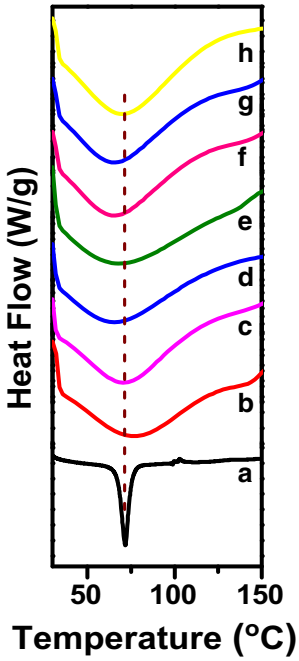

Fig. 3 DSC thermograms of (a) PEO, (b) $PEO_8/LiClO_4$, and PEO8/$LiClO_4$ + x wt% Al-LLZO with (c) $x = 5$, (d) $x = 10$, (e) $x = 15$, (f) $x = 20$, (g) $x = 25$, and (h) $x = 30$

observed at 1130 and 1055 cm^{-1} in PEO disappeared with Li salt. This might be due to the interaction of Li salts with the ethylene oxygen (EO) of PEO.

Figure 2c displays the FTIR spectrum of GCPEM-20 membrane. The addition of garnet oxide displays minor changes in the FTIR spectrum of $PEO_8/LiClO_4$ (Fig. 2b). These minor changes could be attributed to the Van der Waals interaction between the Al-LLZO garnet oxide and the ether oxygen group present in PEO.

Differential scanning calorimetry (DSC)

DSC thermograms of PEO, $PEO_8/LiClO_4$, $PEO_8/LiClO_4$ + x wt% Al-LLZO ($x = 5$, 10, 15, 20, 25, and 30) are displayed in Fig. 3. The sharp endothermic peak at 71.7 °C in Fig. 3a corresponds to the melting of crystalline phase of PEO. On blending with $LiClO_4$, the melting point of PEO in the polymer-lithium salt complex is slightly shifted towards a lower temperature (69.9 °C) as shown in Fig. 3b. When Al-LLZO is introduced into the $PEO_8/LiClO_4$ matrix, the melting takes place at further lower temperatures. The melting temperature (T_m) has been reduced from 71.7 °C for PEO to 63.8 °C for GCPEM-20 membrane. The dispersion of Al-LLZO filler leads to broadening of PEO melting curve as it is clearly visible in Fig. 3c–g. The observed peak broadening and low melting temperatures of composite membranes might be due to the suppression of crystalline nature of PEO. The addition of lithium salt and the garnet oxide decreases the degree of crystallinity of PEO and reaches a lowest value for GCPEM-20 membrane. However, loading beyond 20 wt% Al-LLZO into $PEO_8/LiClO_4$ matrix increases the melting temperature as shown in Fig. 3h.

Table 1 shows the melting temperature (T_m), melting enthalpy (ΔH_m), and degree of crystallinity (χ_c) for PEO, $PEO_8/LiClO_4$, $PEO_8/LiClO_4$ + x wt% Al-LLZO ($x = 5$, 10, 15, 20, 25, and 30). Degree of crystallinity (χ_c) is calculated using Eq. (1):

$$\chi_c = \frac{\Delta H_m}{\Delta H_m^o} \times 100 \quad (1)$$

where ΔH_m is melting enthalpy obtained from the DSC curve and $\Delta H^o{}_m = 213.7$ J g^{-1} is the standard melting enthalpy for PEO [25].

Table 1 reveals that the addition of $LiClO_4$ to polymer matrix decreases the melting temperature and degree of crystallinity. The interaction between the ether oxygen of PEO chain and Li^+ ions prevent the reorganization of polymer chain and decrease the recrystallization of PEO. The addition of Al-LLZO to the $PEO_8/LiClO_4$ further decreases the χ_c and T_m. On the contrary, when the content of Al-LLZO reaches to 25 wt%, the χ_c and T_m increases which may be attributed to the Lewis acid base interaction between the EO atoms of PEO chain and Lewis acid sites on the surface of Al-LLZO.

Table 1 Melting temperature (T_m), melting enthalpy (ΔH_m), and degree of crystallinity (χ_c) for PEO, $PEO_8/LiClO_4$, $PEO_8/LiClO_4 + x$ wt% Al-LLZO ($x = 5$, 10, 15, 20, 25, and 30)

Sample	T_m (°C)	ΔH_m (J/g)	χ_c (%)
PEO	71.7	167.60	78.4
$PEO_8/LiClO_4$	69.9	142.51	66.7
$PEO_8/LiClO_4$ + 5 wt% Al-LLZO	67.8	132.65	62.0
$PEO_8/LiClO_4$ + 10 wt% Al-LLZO	65.9	96.86	45.3
$PEO_8/LiClO_4$ + 15 wt% Al-LLZO	63.9	89.26	42.0
$PEO_8/LiClO_4$ + 20 wt% Al-LLZO	63.8	47.59	22.2
$PEO_8/LiClO_4$ + 25 wt% Al-LLZO	65.8	63.66	29.7
$PEO_8/LiClO_4$ + 30 wt% Al-LLZO	69.8	77.74	36.3

Electrochemical impedance spectroscopy (EIS)

The Li^+ conductivity of the GCPEM was studied by impedance spectroscopy. The ionic conductivity (σ) was calculated from the following relation:

$$\sigma = \frac{l}{RA} \tag{2}$$

where l is the thickness (cm) of the membrane, A is the contact area of electrode with respect to the electrolyte (cm^2), and R is the resistance (ohm) of the sample.

Figure 4a displays the room temperature AC impedance (Cole-Cole) plots of $PEO_8/LiClO_4 + x$ wt% Al-LLZO with $x = 5$, 10, 15, 20, 25, and 30. The impedance plots contain an arc in the high-frequency region followed by a linear tail in the low-frequency region. The appearance of capacitive tail is attributed to the ionically blocking steel electrodes. The total Li^+ conductivity is calculated from the intercept of the arc on the real axis (Z′). The inset in Fig. 4a shows the impedance plot at high-frequency region. Lithium-ion conductivity measurements of prepared GCPEM were performed using Li^+ blocking stainless steel electrodes in the frequency range 20 Hz to 15 MHz. The available high frequency of 15 MHz is not sufficient to get complete semicircle, hence unable to resolve the grain and grain boundary contribution; hence, we presented the total conductivity. The room temperature Li^+ conductivity values for the investigated composite membranes are tabulated in Table 2.

The variation of Li^+ conductivity of GCPEM with the filler content is shown in Fig. 4b. The room temperature Li^+ conductivity initially increases with the Al-LLZO content and reaches a maximized value of 4.40×10^{-4} S cm^{-1} for 20 wt% filler (GCPEM-20). The Al-LLZO filler provides cross-linking centers for the PEO chains giving rise to additional pathways and also hinder the crystallization kinetics of PEO which leads to high Li^+ conduction. As the filler content continues to increase beyond 20 wt%, the room temperature Li^+ conductivity decreases. This might be due to the blocking effect on the conducting pathways of lithium ions resulting from the aggregation of the garnet oxide filler.

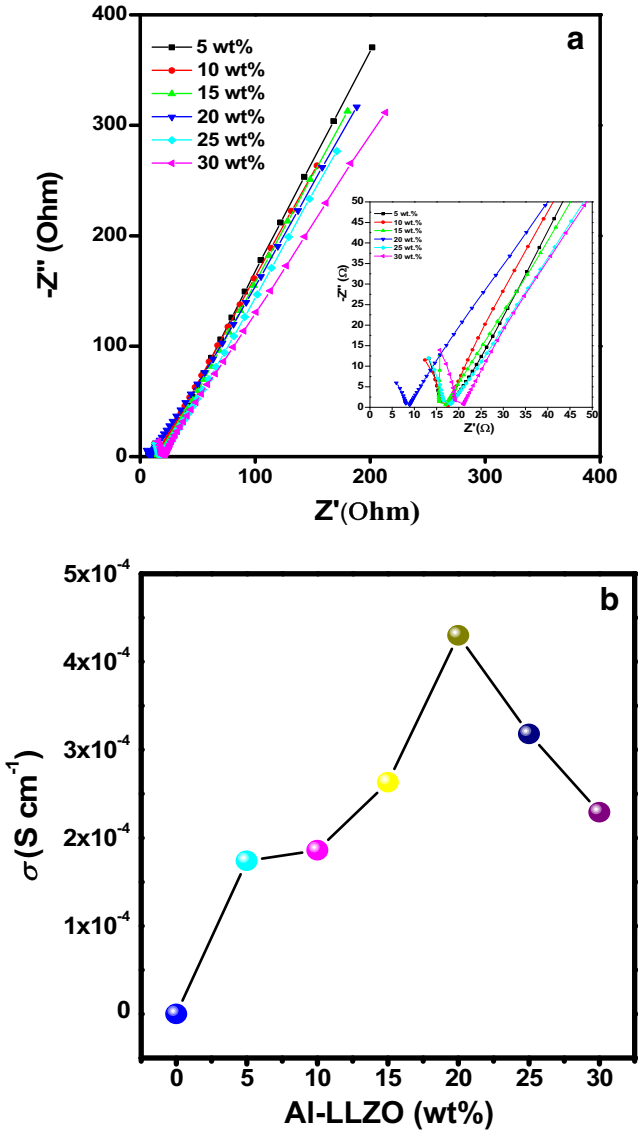

Fig. 4 **a** AC impedance plots of $PEO_8/LiClO_4 + x$ wt% Al-LLZO ($x = 5$, 10, 15, 20, 25, and 30). **b** Ionic conductivity vs. Al-LLZO wt% in $PEO_8/LiClO_4 + x$ wt% Al-LLZO ($x = 0$, 5, 10, 15, 20, 25, and 30)

Table 2 Room temperature (30 °C) total (bulk + grain boundary) Li^+ conductivity of $PEO_8/LiClO_4 + x$ wt% Al-LLZO ($x = 5$, 10, 15, 20, 25, and 30)

Sample	Conductivity (S cm^{-1})
$PEO_8/LiClO_4$ + 5 wt% Al-LLZO	1.74×10^{-4}
$PEO_8/LiClO_4$ + 10 wt% Al-LLZO	2.52×10^{-4}
$PEO_8/LiClO_4$ + 15 wt% Al-LLZO	2.63×10^{-4}
$PEO_8/LiClO_4$ + 20 wt% Al-LLZO	4.40×10^{-4}
$PEO_8/LiClO_4$ + 25 wt% Al-LLZO	2.72×10^{-4}
$PEO_8/LiClO_4$ + 30 wt% Al-LLZO	2.34×10^{-4}

Earlier, Keller et al. pointed out a diminished Li^+ conductivity upon LLZO addition to the PEO: Li matrices which they have carried out at higher percentage of LLZO when compared with our present system [26]. Zheng et al. reported that Li^+ prefer the pathway through the LLZO ceramic phase instead of the PEO-LLZO interface or PEO in PEO composite electrolyte [18]. Hence, the major contributor for the maximized Li^+ conductivity observed in $PEO_8/LiClO_4$ + 20 wt% Al-LLZO might be due to the effect of Al-LLZO addition.

Scanning electron microscope (SEM) and transmission electron microscope (TEM)

SEM image on morphology of $Li_{6.28}Al_{0.24}La_3Zr_2O_{12}$ garnet oxide powder shown in Fig. 5a revealed the uniform distribution of particle size. SEM image of PEO in Fig. 5b revealed an uneven morphology as reported earlier for PEO-based electrolytes prepared by the solution casting method [27]. The scanning electron micrograph of $PEO_8/LiClO_4$complex given in Fig. 5c revealed smooth surface due to addition of lithium salt into the PEO. The smooth surface morphology is closely related to the reduction of PEO crystallinity via interaction between PEO segments and lithium ions. The reduction of crystallinity resulted in highly flexible electrolyte owing to the increased segmental motion of the polymer chains [28]. Figure 5d indicates the effect of dispersion of Al-LLZO garnet filler in the GCPEM-20 membrane.

Figure 5e shows the TEM image of composite polymer membrane containing 20 wt% Al-LLZO garnet oxide filler (GCPEM-20). The darker region in Fig. 5e shows the dispersed Al-LLZO particles into the polymer system. Since the Al-LLZO particle size is small, it can be interposed well between the polymer chains and reduce the crystalline phase of PEO. This indication is also in agreement with XRD as well as DSC results. On the other hand, a large amount of garnet filler can agglomerate and obstruct the ion movement in between the PEO chains.

Figure 5f shows photographic images of the as prepared free standing GCPEM-20 membrane. The addition of garnet filler into the polymer matrix facilitates the free-standing ability to the composite polymer membrane.

Electrochemical stability of the GCPEM-20 membrane

The electrochemical stability of solid polymer electrolytes is a major concern for high-performance lithium batteries. Electrochemical techniques such as cyclic voltammetry (CV) and linear sweep voltammetry (LSV) measurements were carried out for the GCPEM-20 membrane, and its electrochemical stability was evaluated. CV measurements were carried out using two electrodes system Li/GCPEM-20/SS consisting of a stainless steel as working electrode and metallic lithium as reference/counter electrode. From the CV data measured at 70 °C shown in Fig. 6a, it can be clearly seen that that the stripping and a plating of Li/Li^+ in GCPEM-20 membrane was observed at 0 V and the anodic limit was the irreversible oxidation at ~ 4.5 V.

The LSV was carried out between 0 to 5 V at various scan rate (0.1, 5, and 10 mV/s) at room temperature. As presented in Fig. 6, no significant oxidation current was observed until 4.5 V at various scan rates, which shows that the GCPEM-20 membrane was electrochemically stable up to 4.5 V.

Electrochemical performance of Li/GCPEM-20/Li symmetric cell

In order to verify the electrochemical compatibility of GCPEM-20 membrane with metallic lithium, we investigated the symmetric cell performance by staking the GCPEM-20 membrane of area 1.7 cm^2 between two metallic lithium disks of area 1 cm^2 on each inside in an Ar-filled glove box. The cells were rested for 4 h after fabrication. Figure 7a represents the schematic illustration of the fabricated Li/GCPEM-20/Li symmetric cell. The symmetric cell was galvanostatically cycled at constant current of 0.05 mA cm^{-2} with 5-min charging and 5-min discharging time to obtain the voltage profiles under room temperature conditions. A smooth and stable voltage profile was observed with a voltage range of ± 0.005 V. Stable voltage profile indicated that the impedance of GCPEM-20 membrane does not increase under the galvanostatic cycling of cell for extended time duration 65 h.

Bruce and Vincent method was used to provide transference number of the investigated composite [29]. The $t_{Li}{}^+$ is given by the Eq. (3):

$$t_{Li^+} = \frac{I_{ss}(\Delta V - I_0 R_0)}{I_0(\Delta V - I_{ss} R_{ss})} \tag{3}$$

where

ΔV is a small D.C. bias applied to polarize the sample, I_0 is an initial value of current upon polarization with D.C. bias, I_S is a current reached in the steady state for sample polarized with D.C. bias, and R_0 and R_S are resistances of solid electrolyte interface (SEI) before and after polarization. The Li^+ transference number for the prepared $PEO_8/LiClO_4$ is 0.20. The Li^+ transference number for the prepared composite polymer membrane (GCPEM-20) is 0.29.

Electrochemical performance of Li/GCPEM-20/LCO

To demonstrate the practical application as well as performance of as synthesized GCPEM-20, a complete cell (Li/GCPEM-20/LCO) was assembled inside the Ar-filled glove

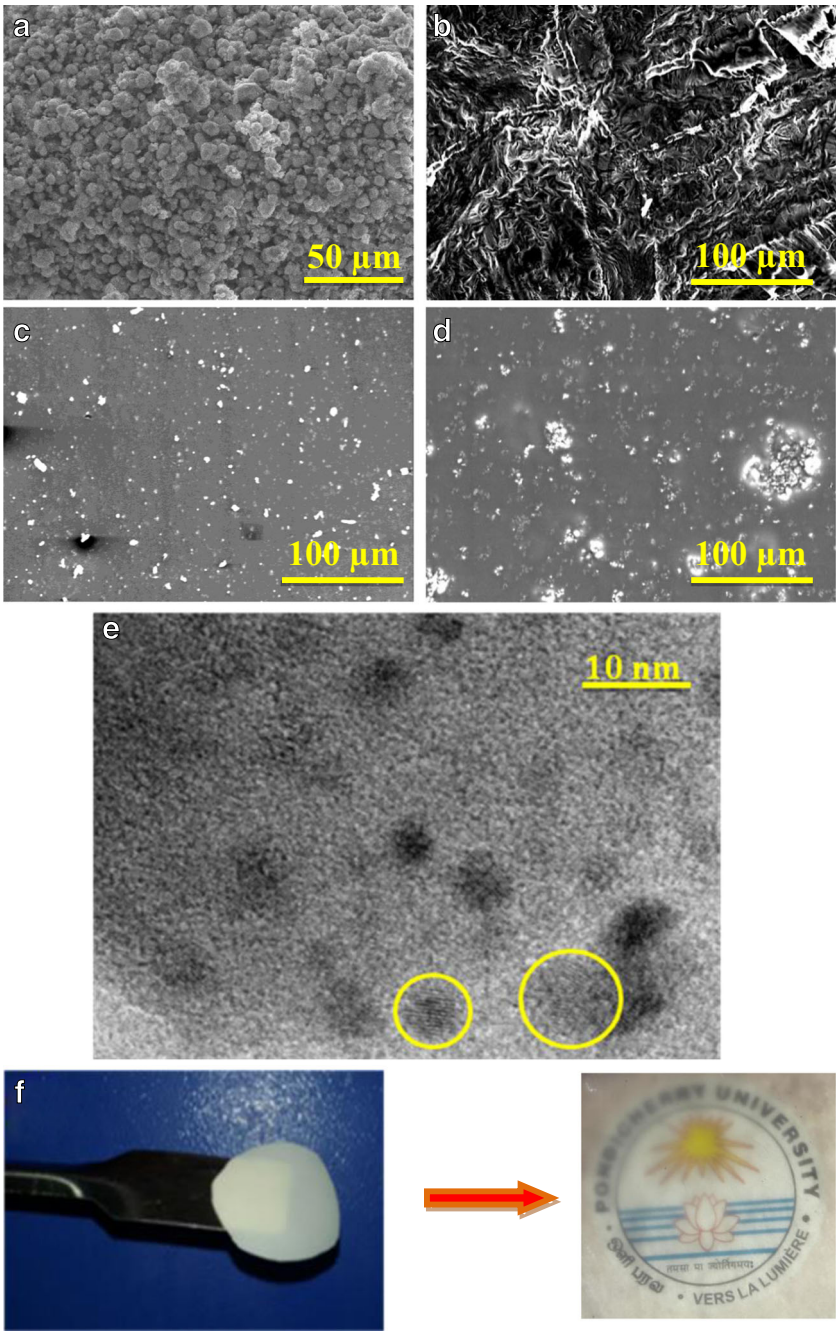

Fig. 5 SEM images of **a** Al-LLZO, **b** PEO, **c** $PEO_8/LiClO_4$, **d** GCPEM-20 membrane, and **e** TEM image of GCPEM-20 membrane. **f** Photographic images of free standing transparent GCPEM-20 membrane

box and galvanostatically cycled at room temperature (25 °C) after the 4 h of cell fabrication. Optimized composite polymer membrane GCPEM-20 was used as an electrolyte whereas $LiCoO_2$ (LCO) and metallic lithium were used as cathode and anode, respectively. The active mass and surface area of the cathode material was 5.6 mg and 1.13 cm^2, respectively. Figure 7b indicates the charge/discharge profiles obtained with the Li/GCPEM-20/LCO. The initial charge/discharge capacity is 146 mAh g^{-1}/142 mAh g^{-1} at 0.06 C-rate. Figure 7c represents the performance of GCPEM-20 based Li/GCPEM-20/LCO coin cell battery. A reversible capacity of above 120 mAh g^{-1} with columbic efficiency of around 96% was obtained at the 30th cycle. There might be several factors responsible for the observed capacity decay. The loss of active material and lithium ions, formation of a SEI in the negative electrode, increased polarization, cell impedance, and temperature are some of the factors affecting the cell performance. We are attempting a detailed post mortem analysis with various experimental techniques to understand this. The GCPEM-20 membrane using Al-LLZO is potentially viable; however, further research is needed to improve the performance of the cell and for faster electrochemical response.

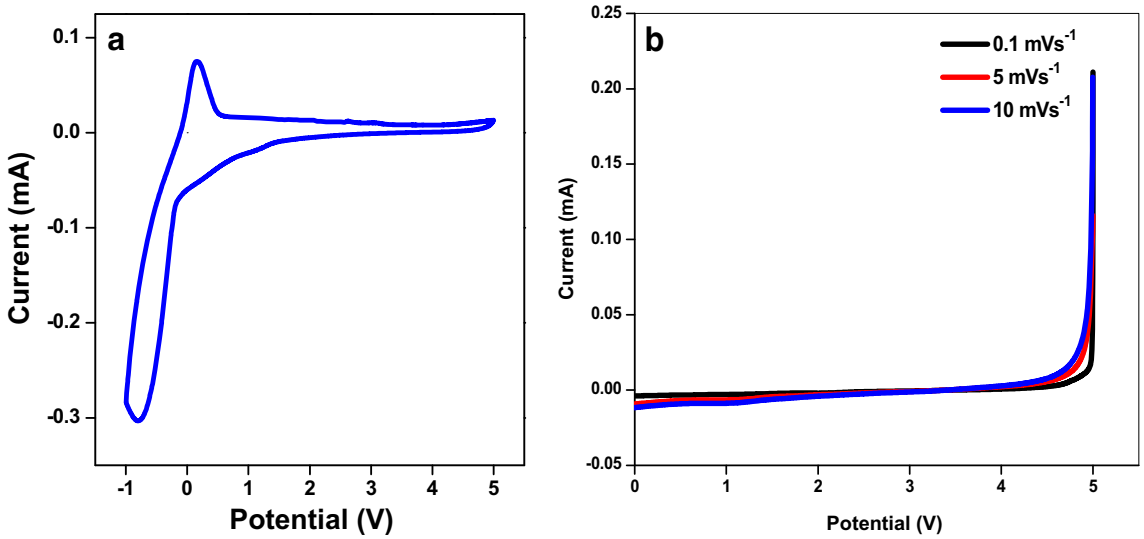

Fig. 6 **a** Cyclic voltammogram of GCPEM-20 membrane. **b** Linear sweep voltammogram of GCPEM-20 membrane

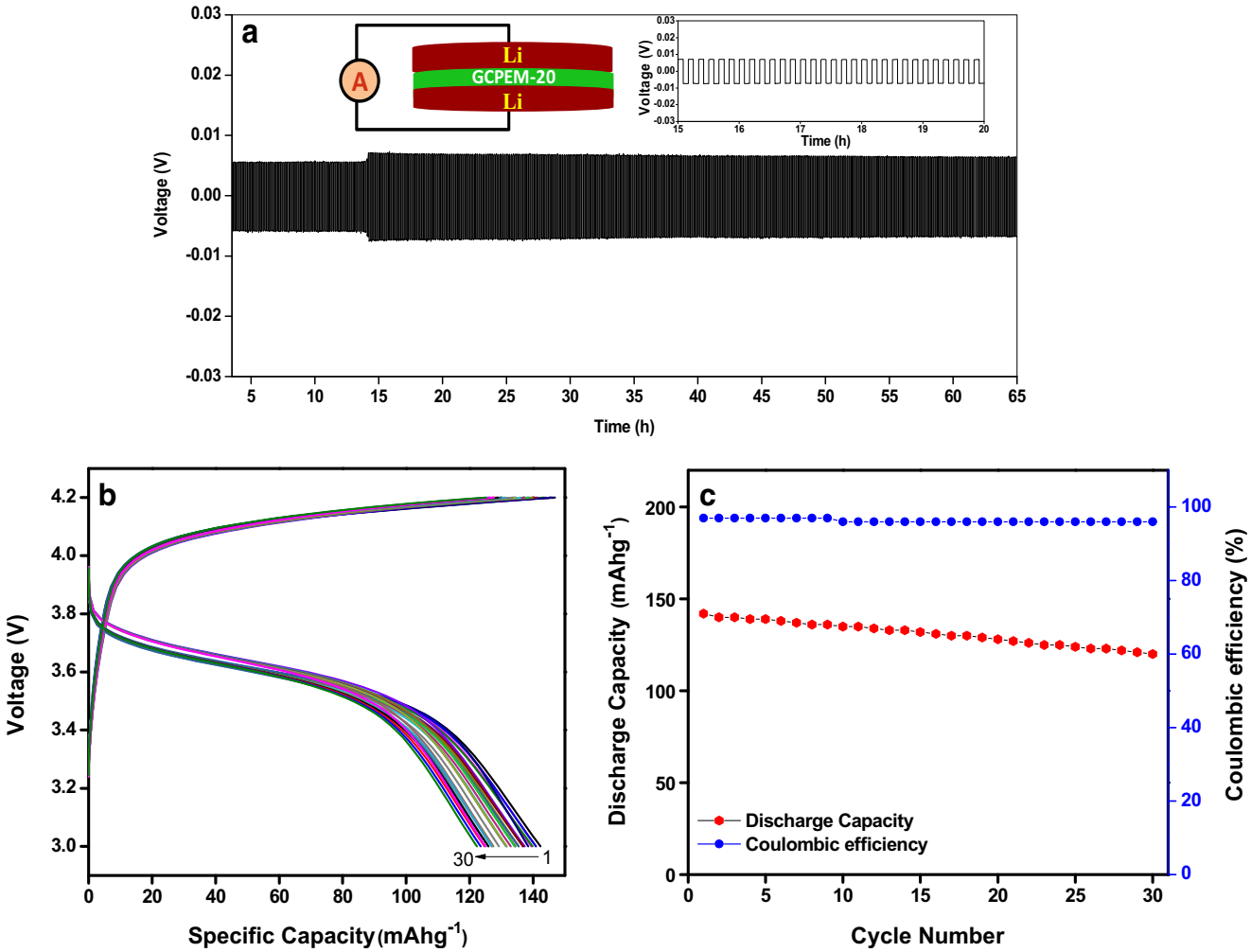

Fig. 7 **a** Voltage profile showing the lithium plating/stripping cycling with a current density of 0.05 mA cm^{-2} for the Li/GCPEM-20/Li symmetric cell at 25 °C. **b** Representative charge/discharge profiles of Li/GCPEM-20/LCO coin cell. **c** Graph illustrating the specific capacity vs number of cycles along with Coulombic efficiency of Li/GCPEM-20/LCO coin cell

Conclusions

Lithium garnet composite polymer electrolyte membrane (GCPEM) based on large molecular weight poly(ethylene oxide) (PEO) complexed with lithium perchlorate ($LiClO_4$) and garnet oxide $Li_{6.28}Al_{0.24}La_3Zr_2O_{12}$ (Al-LLZO) were prepared by standard solution casting method. The coordination between the Al-LLZO garnet oxide and the ether oxygen of the PEO chains led to decrease in crystalline nature of PEO. The Li^+ conductivity investigations revealed an enhanced Li^+ conductivity with the addition of Al-LLZO garnet oxide into the $PEO_8/LiClO_4$ matrix. Maximized room temperature (30 °C) Li^+ conductivity of 4.40×10^{-4} S cm^{-1} was obtained for 20 wt.% Al-LLZO dispersed on $PEO_8/LiClO_4$ (GCPEM-20). Moreover, the cyclic voltammetry (CV) and linear sweep voltammetry (LSV) results confirm that the GCPEM-20 membrane exhibits electrochemical stability greater than 4.5 V. The Li/GCPEM-20/LCO cell delivered an initial discharge specific capacity of 142 mAh g^{-1} with an efficiency of 97% at the first cycle. A reversible capacity of above 120 mAh g^{-1} with columbic efficiency of around 96% was obtained at the 30th cycle at room temperature. The result gives the wide research possibility to improve the C-rate performances, capacity, and cyclability with the GCPEM membrane.

Acknowledgements The authors acknowledge Ministry of Heavy Industries, Government of India (No. 7/1/2013-AEI) and Applied Materials India Pvt. Ltd. for establishing laboratory facilities to carry out part of this work. The authors also acknowledge SERB-DST, New Delhi, India, for the support (EMR/2017/000417). One of the authors (KK) would like to acknowledge UGC-SRF New Delhi (23/12/2012(ii) EU-V), India, towards the financial support to carry out this work.

References

1. Choi JH, Lee CH, Yu JH, Doh CH, Lee SM (2015) Enhancement of ionic conductivity of composite membranes for all-solid-state lithium rechargeable batteries incorporating tetragonal $Li_7La_3Zr_2O_{12}$ into a polyethylene oxide matrix. J Power Sources 274:458–463
2. Inaguma Y, Liquan C, Itoh M, Nakamura T, Uchida T, Ikuta H, Wakihara M (1993) High ionic conductivity in lithium lanthanum titanate. Solid State Commun 86(10):689–693
3. Fu J (1997) Fast Li^+ ion conduction in Li_2O-Al_2O_3-TiO_2-SiO_2-P_2O_2 glass-ceramics. J Am Chem Soc 80(7):1901–1903
4. Kanno R, Murayama M (2001) Lithium ionic conductor Thio-LISICON: the $Li_2SGeS_2P_2S_5$ system. J Electrochem Soc 148(7): A742–A746
5. Hayashi A, Hama S, Minami T, Tatsumisago M (2003) Formation of superionic crystals from mechanically milled Li_2S–P_2S_5 glasses. Electrochem Commun 5(2):111–114
6. Kamaya N, Homma K, Yamakawa Y, Hirayama M, Kanno R, Yonemura M, Mitsui A (2011) A lithium superionic conductor. Nat Mater 10(9):682–686
7. Agrawal RC, Pandey GP (2008) Solid polymer electrolytes: materials designing and all-solid-state battery applications: an overview. J Phys D Appl Phys 41(22):223001
8. Tambelli CC, Bloise AC, Rosario AV, Pereira EC, Magon CJ, Donoso JP (2002) Characterisation of PEO–Al_2O_3 composite polymer electrolytes. Electrochim Acta 47(11):1677–1682
9. Masoud EM, El-Bellihi AA, Bayoumy WA, Mousa MA (2013) Effect of $LiAlO_2$ nanoparticle filler concentration on the electrical properties of PEO–$LiClO_4$ composite. Mater Res Bull 48(3):1148–1154
10. Zhang XW, Wang C, Appleby AJ, Little FE (2002) Characteristics of lithium-ion-conducting composite polymer-glass secondary cell electrolytes. J Power Sources 112(1):209–215
11. Kesavan K, Mathew CM, Rajendran S, Subbu C, Ulaganathan M (2015) Solid polymer blend electrolyte based on poly (ethylene oxide) and poly (vinyl pyrrolidone) for lithium secondary batteries. Braz J Phys 45(1):19–27
12. Croce F, Appetecchi GB, Persi L, Scrosati B (1998) Nanocomposite polymer electrolytes for lithium batteries. Nature 394(6692):456–458
13. Wieczorek W, Such K, Przyłuski J, Floriańczyk Z (1991) Blend-based and composite polymer solid electrolytes. Synth Met 45(3):373–383
14. Fullerton-Shirey SK, Maranas JK (2010) Structure and mobility of PEO/$LiClO_4$ solid polymer electrolytes filled with Al_2O_3 nanoparticles. J Phys Chem C 114(20):9196–9206
15. Tang Z, Wang J, Chen Q, He W, Shen C, Mao XX, Zhang J (2007) A novel PEO-based composite polymer electrolyte with absorptive glass mat for li-ion batteries. Electrochim Acta 52(24):6638–6643
16. Zheng J, Tang M, Hu YY (2016) Lithium ion pathway within Li7La3Zr2O12-polyethylene oxide composite electrolytes. Angew Chem 128(40):12726–12730
17. Yue L, Ma J, Zhang J, Zhao J, Dong S, Liu Z, Chen L (2016) All solid-state polymer electrolytes for high-performance lithium ion batteries. Energy Storage Mater 5:139–164
18. Zheng J, Tang M, Hu YY (2016) Lithium ion pathway within $Li_7La_3Zr_2O_{12}$-polyethylene oxide composite electrolytes. Angew Chem Int Ed 55(40):12538–12542
19. Buvana P, Vishista K, Shanmukaraj D, Murugan R (2017) Lithium garnet oxide dispersed polymer composite membrane for rechargeable lithium batteries. Ionics 23(3):541–548
20. Deviannapoorani C, Ramakumar S, Janani N, Murugan R (2015) Synthesis of lithium garnets from $La_2Zr_2O_7$ pyrochlore. Solid State Ionics 283:123–130
21. Dey A, Karan S, De SK (2009) Effect of nanofillers on thermal and transport properties of potassium iodide–polyethylene oxide solid polymer electrolyte. Solid State Commun 149(31–32): 1282–1287
22. Dhivya L, Karthik K, Ramakumar S, Murugan R (2015) Facile synthesis of high lithium ion conductive cubic phase lithium garnets for electrochemical energy storage devices. RSC Adv 5(116): 96042–96051
23. Fahmi EM, Ahmad A, Hamzah H, Rahman MYA (2013) Preparation and characterization of PEO-NiO-$LiCF_3SO_3$ composite polymer electrolyte. Int J Electroact Mater 1(1):2–8
24. Masoud EM, El-Bellihi AA, Bayoumy WA, Mousa MA (2013) Organic–inorganic composite polymer electrolyte based on PEO–$LiClO_4$ and nano-Al_2O_3 filler for lithium polymer batteries: dielectric and transport properties. J Alloys Compd 575: 223–228
25. Xi J, Qiu X, Cui M, Tang X, Zhu W, Chen L (2006) Enhanced electrochemical properties of PEO-based composite polymer electrolyte with shape-selective molecular sieves. J Power Sources 156(2):581–588

26. Keller M, Appetecchi GB, Kim GT, Sharova V, Schneider M, Schuhmacher J, Roters A, Passerini S (2017) Electrochemical performance of a solvent-free hybrid ceramic-polymer electrolyte based on $Li_7La_3Zr_2O_{12}$ in $P(EO)_{15}$LiTFSI. J Power Sources 353:287–297
27. Chu PP, Reddy MJ (2003) Sm_2O_3 composite PEO solid polymer electrolyte. J Power Sources 115(2):288–294
28. Fahmi EM, Ahmad A, Nazeri NNM, Hamzah H, Razali H, Rahman MYA (2012) Effect of $LiBF_4$ salt concentration on the properties of poly (ethylene oxide)-based composite polymer electrolyte. Int J Electrochem Sci 7:5798–5804
29. Bruce PG, Vincent CA (1987) Steady state current flow in solid binary electrolyte cells. J Electroanal Chem Interfacial Electrochem 225(1-2):1–17